SOFT SENSOR FOR ON-LINE MONITORING OF PARTICLE SIZES IN MINIEMULSION POLYMERIZATION

Luis A. Clementi[a,b], Jorge R. Vega[a,b], Luis M. Gugliotta[b]

[a]*Fac. Reg. Santa Fe, Universidad Tecnológica Nacional, Lavaise 610, 3000 Santa Fe, Argentina,*
http://www.frsf.utn.edu.ar/

[b]*INTEC, Univ. Nac. del Litoral y CONICET, Guemes 3450, 3000 Santa Fe, Argentina,*
director@intec.unl.edu.ar, http://www.intec.unl.edu.ar/

Keywords: Polymeric Colloid, Inverse Problems, Tikhonov Regularization, General Regression Neural Networks

Abstract. This paper proposes a soft-sensor (SS) for on-line monitoring the droplet/particle size distribution (PSD) in miniemulsion polimerizations. The SS utilizes turbidity measurements and a global particle refractive index (PRI) estimated on the basis of the instantaneous polymer conversion and the PRIs of the monomer and the polymer. The proposed method requires solving an ill-conditioned inverse problem (ICIP). Two different approaches are proposed for solving the ICIP: i) a Tikhonov regularization (TR), and ii) a General Regression Neural Network (GRNN). Both approaches are evaluated on the basis of simulated examples corresponding to a styrene miniemulsion polymerization. For unimodal PSDs, both TR and GRNN produce acceptable estimates of the average diameters of the PSD along the polymerization. The TR method produces PSDs with spurious peaks, while the GRNN allows better estimates. For bimodal PSDs both methods produce acceptable average diameters but erroneous PSDs. Simulation results suggest that the proposed method is a robust tool for on-line monitoring of the average diameters in miniemulsion polymerizations.

1 INTRODUCTION

A polymer colloid (or latex) is normally constituted by submicrometric polymer particles dispersed in an aqueous medium. Latexes are typically used in the production of paints, inks, coatings, adhesives, immunoassay kits, drugs delivery systems, etc. Synthetic latexes are mostly obtained through aqueous phase microemulsion, miniemulsión, emulsion, and dispersion polymerization processes (Gugliotta et al., 2010). Particularly, miniemulsion polymerization involves the utilization of a surfactant/stabilizer system to produce stable monomer droplets (the miniemulsion itself) of small sizes (normally, 10 nm – 500 nm) (Schork et al., 2005). After the initiation (either outside or inside the droplets) the polymerization is mainly carried out within the monomer droplets. Along a miniemulsion polymerization the dispersed droplets and particles can exhibit a wide variety of monomer/polymer ratios since the initiation of the polymerization is not instantaneous in all monomer droplets. Miniemulsion polymerization represents an alternative for the synthesis of hybrid latexes; and enables the incorporation of a hydrophobic component into the polymer particles in a single step process, without requiring its diffusion through the aqueous phase since the miniemulsion droplets can be generated containing all the components to be incorporated in the synthesized material (Minari et al., 2009; Ronco et al., 2013).

The particle size distribution (PSD) is a morphological characteristic of primary importance in several particulate systems including miniemulsions, emulsions, suspensions and dispersions. In the particular case of a latex, the PSD affects the end-use properties (e.g., rheological, mechanical, physical) of the material when used as an adhesive, a paint, an ink, or a coating. Also, the PSD affects the growth, and the interaction of the particles along heterogeneous polymerizations (Gugliotta et al., 2010). For such reason, the accurate knowledge of the PSD is necessary not only for the characterization of the final products, but also for the understanding of the physicochemical mechanisms that take place in the course of miniemulsion polymerizations. Additionally, on-line monitoring of the PSD along miniemulsion polymerizations is important for the developing of control strategies.

On-line monitoring of the PSD is difficult due to the lack of a sensor for measuring the PSD in the polymerization reactor medium. Alternatively, the PSD can be estimated through an indirect method that involve: i) the measurement of a given physical property of the particles, and ii) the resolution of an inverse problem (IP) (Tikhonov and Arsenin, 1977) on the basis of a mathematical model that relate the measurements with the PSD. At present, a light scattering (LS) based-method, such as turbidimetry (T), is a powerful technique for estimating the PSD of a latex. In fact, T is fast, simple, and absolute (in the sense that it does not require a previous calibration); and besides it does not produce sample damages (Gugliotta et al., 2010).

Main definitions concerning PSDs of homogeneous spherical particles were reviewed by Gugliotta et al. (2010). We shall call $f(D_i)$ the discrete number PSD. The ordinates of $f(D_i)$ represent the number (or number concentration) of particles contained in the diameter interval $[D_i , D_i + \Delta D]$ ($i = 1, \ldots, I$), being ΔD a regular partition of the D axis. For a given discrete PSD, several average diameters, that we shall call $\overline{D}_{a,b}$, can be defined as follows:

$$\overline{D}_{a,b} = \left(\frac{\displaystyle\sum_{i=1}^{I} f(D_i)\, D_i^a}{\displaystyle\sum_{i=1}^{I} f(D_i)\, D_i^b} \right)^{\frac{1}{a-b}} \tag{1}$$

For example, $\overline{D}_{1,0} = \overline{D}_n$ is the number-average diameter, and $\overline{D}_{4,3} = \overline{D}_w$ is the weight-average diameter.

In a T experiment, the attenuation of a light beam while traveling through a dilute sample is measured as a function of the light wavelength, λ_j ($j = 1, \ldots, J$), and the turbidity spectrum, $\tau(\lambda_j)$, is calculated as follows:

$$\tau(\lambda_j) = (1/\ell)\ln[I_0(\lambda_j)/I_t(\lambda_j)] \tag{2}$$

where ℓ is the optical path length, and $I_0(\lambda_j)$ and $I_t(\lambda_j)$ are the intensity of the incident and the emerging light beams. In absence of multiple scattering (i.e., when the light scattered by a particle does not interact with any other particle), and assuming spherical and homogenous particles, the PSD $f(D_i)$ is related with the T measurement $\tau(\lambda_j)$ as follows (Gugliotta et al., 2010):

$$\tau(\lambda_j) = k_\tau \sum_{i=1}^{I} Q_{ext}[D_i, \lambda_j, n_m(\lambda_j), n_p(\lambda_j)]\, D_i^2\, f(D_i) \quad ; \quad j = 1, \ldots, J \tag{3}$$

where k_τ is a known experimental constant, and $Q_{ext}[D_i, \lambda_j, n_m(\lambda_j), n_p(\lambda_j)]$ is the light extinction by a particle of diameter D_i and refractive index $n_p(\lambda_j)$ immersed in a non-absorbing medium of refractive index $n_m(\lambda_j)$ at the wavelength λ_j, and is calculated through the Mie scattering theory (Bohren and Huffman, 1983).

For homogeneous particles composed of two different species, the particle refractive index (PRI) $n_p(\lambda_j)$ can be calculated as follows (Iulian et al., 2010):

$$n_p(\lambda_j) = \varphi_1\, n_{p,1}(\lambda_j) + \varphi_2\, n_{p,2}(\lambda_j) \tag{4}$$

where φ_1 and φ_2 are the volume fraction of species with PRI $n_{p,1}(\lambda_j)$ and $n_{p,2}(\lambda_j)$, respectively.

Equation (3) represent a system of J linear equation with I unknowns (the ordinates of the PSD), that can be rewritten in a matrix form, as follows:

$$\boldsymbol{\tau} = k_\tau\, \mathbf{Q}\, \mathbf{f} \tag{5}$$

where $\boldsymbol{\tau}$ (J×1) and $\mathbf{f}$ (I×1) are vectors with components $\tau(\lambda_j)$ and $f(D_i)$, respectively, and $\mathbf{Q}$ (J×I) is the matrix with the (j,i)-th component given by $Q_{ext}[D_i, \lambda_j, n_m(\lambda_j), n_p(\lambda_j)]\, D_i^2$. The PSD $\mathbf{f}$ can be estimated from $\boldsymbol{\tau}$ by inverting Eq. (5). To this effect, matrix $\mathbf{Q}$ is calculated through the Mie scattering theory (Bohren and Huffman, 1983) and the PRI $n_p(\lambda_j)$ must be accurately known. Inversion of Eq. (5) is known to be an "ill-conditioned" inverse problem (ICIP); i.e., small perturbation caused by experimental noise or uncertainties in the PRI can lead to important deviations in the estimated PSD.

When the colloid exhibits particles of different composition (and thus different PRIs), as in

the case of a miniemulsion polymerization, Eq. (5) can be generalized as follows:

$$\boldsymbol{\tau} = k_\tau \left[\mathbf{Q}_1 \, \mathbf{f}_1 + \mathbf{Q}_2 \, \mathbf{f}_2 + \cdots + \mathbf{Q}_L \, \mathbf{f}_L \right] \tag{6}$$

where $\mathbf{Q}_l$ (J×I) (l = 1, ..., L) is the l-th matrix with components $Q_{ext}[D_i, \lambda_j, n_m(\lambda_j), n_{p,l}(\lambda_j)] D_i^2$ corresponding to the particle population with a fixed composition and PRI $n_{p,l}(\lambda_j)$, and $\mathbf{f}_l$ (I×1) is the corresponding PSD for a given particle composition. Note that the global PSD is given by:

$$\mathbf{f} = \mathbf{f}_1 + \mathbf{f}_2 + \cdots + \mathbf{f}_N \tag{7}$$

On line monitoring of PSDs by T has been scarcely studied in the literature. Moreover, most papers restrict their study to analyze the sensitivity of T measurements to changes in the characteristics of the colloid rather than proposing methods for estimating the PSD. For example, Chicoma et al. (2011) and Higgins et al. (2003) observed meaningful sensitivity of T measurements along the synthesis of polymeric particles and the production of pharmaceutical drug nanoparticles, respectively. Brandolin et al. (1991) utilized simulated examples to investigate the sensitivity of operative parameters (for example, sample time, latex concentration, light wavelength, etc.) on estimated PSDs obtained by inverting Eq. (5) along emulsion polymerization of styrene. Kiparissides (1980) investigated the on-line monitoring of continuous emulsion polymerization of vinyl-acetate through T measurements. In its work, T at a single wavelength (350 nm) was able to detect the beginning of the polymerization and whether the system reached a steady state or exhibited oscillations. Other authors have utilized alternative light scattering measurements such dynamic light scattering (DLS) and multiangle static light scattering (MALS) for on-line monitoring of average diameters and PSDs along heterogeneous polymerizations (Çatalgis-Giz et al., 2003; Alb et al., 2006; Alb and Reed, 2008). As far as the authors are aware, monitoring of miniemulsion polymerization on the basis of light scattering techniques has not been investigated yet.

In this paper a novel method is proposed for on-line monitoring of the PSD along a miniemulsion polymerization on the basis of T measurements. The method is evaluated through a simulated example corresponding to an aqueous phase miniemulsion polymerization of styrene with PSDs of different average diameters. A Tikhonov regularization method and a general regression neural network are compared as tools for solving the involved ICIP. All the computer work was carried out in Matlab.

2 THE PROPOSED METHOD

On-line estimation of the global PSD along a miniemulsion polymerization through the mathematical model of Eq. (6) and (7) is difficult because the droplets and particles exhibit a wide variety of unknown compositions (and thus, unknown PRIs). In consequence, matrixes $\mathbf{Q}_l$ in Eq. (6) cannot be calculated. An approximated estimation method is proposed in what follows.

Consider the instantaneous polymer conversion, $x(t)$, at each time t, defined as:

$$x(t) = \frac{M_0 - M(t)}{M_0} \tag{8}$$

where M_0 and $M(t)$ are the initial and instantaneous mass concentration of the monomer, respectively. From $x(t)$, the global instantaneous volume fractions of monomer and polymer,

$\varphi_{Mon}(x)$ and $\varphi_{Pol}(x)$, respectively, can be calculated as follows:

$$\varphi_{Mon}(x) = \frac{\dfrac{(1-x)}{\rho_{Mon}}}{\dfrac{(1-x)}{\rho_{Mon}} + \dfrac{x}{\rho_{Pol}}} = 1 - \varphi_{Pol}(x) \tag{9a}$$

$$\varphi_{Pol}(x) = \frac{\dfrac{x}{\rho_{Pol}}}{\dfrac{(1-x)}{\rho_{Mon}} + \dfrac{x}{\rho_{Pol}}} = 1 - \varphi_{Mon}(x) \tag{9b}$$

where ρ_{Mon} and ρ_{Pol} are the known densities of the monomer and the polymer, respectively. Then, a "global" PRI, $n_{p,g}(\lambda_j)$, can be obtained from Eq. (4):

$$n_{p,g}(\lambda_j, x) = \varphi_{Mon}(x)\, n_{p,Mon}(\lambda_j) + \varphi_{Pol}(x)\, n_{p,Pol}(\lambda_j) \tag{10}$$

where $n_{p,Mon}(\lambda_j)$ and $n_{p,Pol}(\lambda_j)$ are the known PRIs of the monomer and the polymer, respectively. Then, from $n_{p,g}(\lambda_j,x)$ the turbidity mathematical model of Eq. (5) can be utilized for estimating a global PSD at each conversion, x. Note that, Eq. (10) implicitly assumes that all particles have a common monomer/polymer composition at each x.

The proposed method for estimating the global PSD can be summarized in the following steps:

i) Measurement of the turbidity spectrum, $\tau(\lambda_j)$ ($j = 1, \dots, J$).
ii) Measurement of the instantaneous polymer conversion x.
iii) Calculation of the global PRI $n_{p,g}(\lambda_j, x)$ from Eqs. (9) and (10).
iv) Calculation of the matrix $\mathbf{Q}$ of Eq. (5) on the basis of $n_{p,g}(\lambda_j, x)$.
v) Solution of the ICIP of Eq. (5) for estimating the global PSD $\mathbf{f}$ [or equivalently $f(D_i)$].

In what follows, two different methods for solving the ICIP are described.

2.1 Tikhonov Regularization Method

The first order Tikhonov regularization method for solving the ICIP of Eq. (5) can be written as the following optimization problem (Tikhonov and Arsenin, 1977):

$$\min_{\hat{\mathbf{f}}} \left\{ \left\| \boldsymbol{\tau} - k_\tau\, \mathbf{Q}\, \hat{\mathbf{f}} \right\|^2 + \alpha \left\| \hat{\mathbf{f}} \right\|^2 \right\}; \quad \hat{f}(D_i) \geq 0 \tag{11}$$

where $\hat{\mathbf{f}}$ (I×1) is a vector whose components are the ordinates of the estimated PSD, $\hat{f}(D_i)$; $\mathbf{Q}$ is the matrix obtained through the Mie scattering theory (Bohren and Huffman, 1983) on the basis of the estimated global PRI, $n_{p,g}(\lambda_j, x)$; α is the regularization parameter; and the symbol $\| \cdot \|$ indicates the 2-norm of a vector. In Eq. (11), the selection of the regularization parameter is critical. Small values of α produce PSDs exhibiting several spurious peaks. On

the other hand, high values of α produce excessively broad PSDs. In general, α depends on: i) the degree of ill-conditioning of the inverse problem (i.e. the condition number of the matrix **Q**); and ii) the measurement noise level. There are a variety of criteria to determine the optimum value of the regularization parameter (Aster et al., 2005). In this work, the L-curve technique is utilized (Hansen and O'Leary, 1993). Computer programs for solving the optimization problem of Eq. (11) were developed based on the regularization tools reported by Hansen (1994).

2.2 General Regression Neural Network

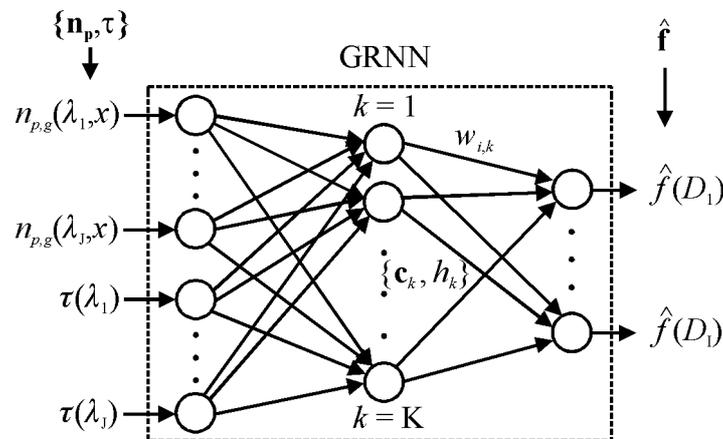Figure 1) presents a scheme of the utilized general regression neural network (GRNN).

Figure 1: Schematic representation of the utilized GRNN

The GRNN involves: 2J inputs, the components of the global PRI vector $\mathbf{n_p} = [n_{p,g}(\lambda_1,x),\cdots,n_{p,g}(\lambda_J,x)]$ and the measurement vector $\boldsymbol{\tau}$; I outputs, the components of the estimated PSD vector **f**; an input layer with 2J neurons; an output layer with I neurons; and a hidden layer with K neurons (Haykin, 1999). The *k*-th neuron in the hidden layer receives the vector $[\mathbf{n_p}\ \boldsymbol{\tau}]$ as input and produces an scalar output of amplitude h_k given by:

$$h_k = \frac{1}{\sigma_k \sqrt{2\pi}} e^{-\frac{\left\| [\mathbf{n_p}\ \boldsymbol{\tau}] - \mathbf{c}_k \right\|^2}{2\sigma_k^2}} \ ; \quad k = 1, \ldots, \text{K}. \tag{12}$$

where $\left\| [\mathbf{n_p}\ \boldsymbol{\tau}] - \mathbf{c}_k \right\|$ represent the distance between the vector $[\mathbf{n_p}\ \boldsymbol{\tau}]$ (2J×1) and the center $\mathbf{c}_k$ (2J×1) of the *k-th* neuron in the hidden layer; and σ_k is the so-called smoothness parameter associated with the *k-th* neuron. From h_k, the components $\hat{f}(D_i)$ ($i = 1, \ldots$I) of the output $\hat{\mathbf{f}}$ of the GRNN are calculated as follows:

$$\hat{f}(D_i) = \sum_{k=1}^{\text{K}} w_{i,k}\ h_k \ ; \quad i = 1, \ldots, \text{I}. \tag{13}$$

where $w_{i,k}$ is the weight coefficient of the connection between the *k-th* hidden neuron and the *i-th* output neuron.

2.2.1 Training of the GRNN

The center of each hidden neuron $\mathbf{c}_k$ and the weight of their connections with the output layer $\mathbf{w}_k = (w_{1,k}, \cdots, w_{I,k})$ are selected by training the GRNN. To this effect, a set of K pairs $\{[\mathbf{n}_{\mathbf{p},k} \ \boldsymbol{\tau}_k] \ , \mathbf{f}_k\}$ (the training patterns) are presented to the GRNN. The training of a GRNN is fast and simple (Specht, 1993). The center of the *k-th* hidden neuron is chosen as $\mathbf{c}_k = [\mathbf{n}_{\mathbf{p},k} \ \boldsymbol{\tau}_k]$, and the weight coefficients of their connections with the output layer are chosen as $\mathbf{w}_k = \mathbf{f}_k$. Consequently, from Eq. (13), the output of the GRNN produces the following PSD estimate:

$$\hat{f}(D_i) = \sum_{k=1}^{K} h_k \ f_k(D_i); \quad i = 1, \dots, I. \tag{14}$$

where:

$$h_k = \frac{1}{\sigma_k \sqrt{2\pi}} e^{-\frac{\left\| [\mathbf{n}_{\mathbf{p}} \ \boldsymbol{\tau}] - [\mathbf{n}_{\mathbf{p},k} \ \boldsymbol{\tau}_k] \right\|^2}{2 \, \sigma_k^2}} \quad ; \quad k = 1, \dots, K. \tag{15}$$

According to Eq. (14), the output of the GRNN $\hat{\mathbf{f}}$ results the linear combination of the training patterns $\mathbf{f}_k$. Note from Eq. (15) that the coefficient h_k in the linear combination of Eq. (14) becomes larger when the center $\mathbf{c}_k = [\mathbf{n}_{\mathbf{p},k} \ \boldsymbol{\tau}_k]$ is closer to the input $[\mathbf{n}_{\mathbf{p}} \ \boldsymbol{\tau}]$. Thus, the output $\hat{\mathbf{f}}$ is mostly defined by those training patterns $\mathbf{f}_k$ that exhibit a small distance $\left\| [\mathbf{n}_{\mathbf{p}} \ \boldsymbol{\tau}] - \mathbf{c}_k \right\| = \left\| [\mathbf{n}_{\mathbf{p}} \ \boldsymbol{\tau}] - [\mathbf{n}_{\mathbf{p},k} \ \boldsymbol{\tau}_k] \right\|$.

For training the GRNN of Fig. 1), a set of K = 283,866 pairs $\{[\mathbf{n}_{\mathbf{p}} \ \boldsymbol{\tau}] \ , \mathbf{f}\}$ were utilized. Each pair was generated as follows:

i) First, a global PSD $f(D_i)$ (or $\mathbf{f}$) was generated on the basis of an exponentially modified Gaussian (EMG) distribution for given values of the average diameter ($\overline{D}_f$), standard deviation (σ_f), and decay constant of the exponential component (τ_f), as follows:

$$f(D_i) = \frac{\Delta D}{\sqrt{2\pi}\sigma_f} \exp\left[-\frac{(D_i - \overline{D}_f)^2}{2 \, \sigma_f^2} \right] * \frac{\exp(-D_i / \tau_f)}{\tau_f / \Delta D} \tag{16}$$

where the symbol '*' stands for convolution product.

ii) A conversion x was selected, and the global PRI $n_{p,g}(\lambda_j, x)$ (or $\mathbf{n_p}$) was calculated through Eq. (10).

iii) The turbidity measurement $\tau(\lambda_j)$ (or $\boldsymbol{\tau}$) was calculated through Eq. (5) on the basis of $f(D_i)$, and the global PRI $n_{p,g}(\lambda_j, x)$.

Steps i) to iii) were implemented for increasing conversions x from 0 to 1, at intervals of 0.02; average diameters $\overline{D}_f$ from 150 nm to 600 nm, at intervals of 10 nm; standard

deviations σ_f from 15 nm to 65 nm, at intervals of 5 nm; and exponential decays τ_f from 15 nm to 65 nm, at intervals of 5 nm. Finally, the GRNN was trained on the basis of the generated pairs. The choice of EMG as basis of the training pattern enables the approximation of a wide variety of different distributions (e.g. Gaussian, normal-logarithmic, etc).

2.2.2 Selection of the smoothness parameter σ_k

The smoothness parameter σ_k affects the selectivity of each hidden neuron. A small σ_k typically produces a highly selective GRNN; i.e., only those neurons with a small norm $\left\| [\mathbf{n_p}\ \boldsymbol{\tau}] - [\mathbf{n}_{\mathbf{p},k}\ \boldsymbol{\tau}_k] \right\|$ meaningfully contribute to the output $\hat{\mathbf{f}}$. On the contrary, a high σ_k produces a less selective GRNN, and therefore neurons with larger distances $\left\| [\mathbf{n_p}\ \boldsymbol{\tau}] - [\mathbf{n}_{\mathbf{p},k}\ \boldsymbol{\tau}_k] \right\|$ will also contribute to the output.

Several methods have been proposed for selecting σ_k (Specht, 1991; Zhong et al., 2005). In this work, a common value of σ_k was used for all the hidden neurons, and was selected according to the "Holdout" method proposed by Specht (1991). To this effect, 10,000 patterns were randomly selected and removed from the original set of 283,866 training patterns. Therefore, the GRNN training (see section 2.2.1) was carried out on the basis of the remaining 273,866 patterns and σ_k was selected by solving the following optimization problem:

$$\min_{\sigma_k}\left(\sum_{k=1}^{10,000} \left\| \mathbf{f}_k - \hat{\mathbf{f}}_k \right\| \right) \tag{17}$$

where $\hat{\mathbf{f}}_k$ is the estimated PSD for the *k-th* removed pattern. According to the "Holdout" method, σ_k is chosen as the value that best reproduces the PSD of the 10,000 removed patterns. The advantage of this method is the simplicity for its implementation and automation.

3   ANALISYS OF SIMULATED EXAMPLES

Consider a simplified model of a miniemulsion polymerization of Styrene. The simulated sample consists of a blend of 10 different species: i) the initial miniemulsion (i.e. droplets of pure Styrene in which conversion is x_0=0); ii) hybrid particles (i.e. particles with monomer and polymer) exhibiting partial conversion of x_1=1/9, x_2=2/9, …, x_8=8/9; and iii) pure polystyrene particles (in which conversion is x_9=1).

Species with x_0=0 exhibits a Normal-Logarithmic PSD, $g_0(D_i)$ [Fig. 2]] defined in the range [50 nm – 700 nm] at regular interval of ΔD = 1 nm and given by:

$$g_0(D_i) = \frac{\Delta D}{D_i\, \sigma \sqrt{2\pi}} \exp\left[-\frac{[\ln(D_i / \overline{D}_0)]^2}{2\sigma^2} \right] \tag{18}$$

where $\overline{D}_0$ = 300 nm is the average diameter and σ = 0.20 is the standard deviation. For the species with $x > 0$, a particle contraction is expected since the density of polystyrene (ρ_{pSt} = 1.05 g/cm^3) is larger than the density of Styrene (ρ_{St} = 0.909 g/cm^3). Thus, the PSD for the species with $x_l > 0$, $g_l(D_i)(l$ = 1, …, 9), were simulated from Eq. (18) assuming the corresponding contracted average diameter:

$$\overline{D}_l = [\rho_{St} / \rho_l(x_l)]^{1/3} \, \overline{D}_0 \, ; \, (l = 1, \, ..., \, 9) \tag{19}$$

with:

$$\rho_l(x_l) = \varphi_{St}(x_l) \, \rho_{St} + \varphi_{pSt}(x_l) \, \rho_{pSt} \, ; \, (l = 1, \, ..., \, 9) \tag{20}$$

where $\rho_l(x_l)$ is the density of particles corresponding to species with conversion x_l; and $\varphi_{St}(x_l)$ and $\varphi_{pSt}(x_l)$ are the volume fractions of styrene and polystyrene for the specie with conversion x_l, respectively, and were obtained from Eqs. (9a) and (9b). Note that for pure polystyrene particles (i.e. with $x_9 = 1$) it results $\overline{D}_9 = [\rho_{St} / \rho_{pSt}]^{1/3} \, \overline{D}_0$. Figure 2 compare the normalized (to equal area) PSDs $g_l(D_i)$ ($l = 0, \, ..., \, 9$).
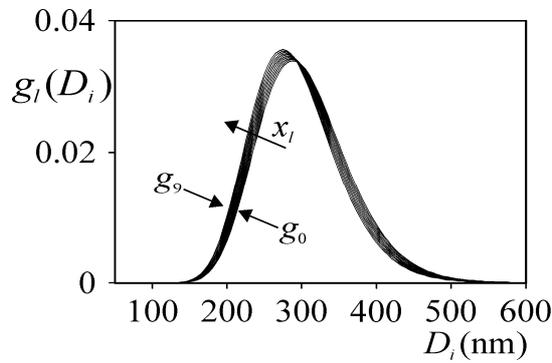

Figure 2: Normalized size distributions $g_l(D_i)$ ($l = 0, \, ..., \, 9$) for the species with conversions $x_l = 0, \, 1/9, \, 2/9, \, ..., \, 1$

Four examples (EX. 1, EX. 2, EX. 3 and EX. 4) were considered by assuming the number concentrations of each species, c_l, that are presented in Table 1. The aim of EX. 1, EX. 2 and EX. 3 is to simulate several stages of a miniemulsion polymerization. EX. 1 corresponds to the initial stage of the polymerization in which only the species with small conversion x_l are present. EX. 2 corresponds to the middle stage in which all species are present. EX. 3 corresponds to the final stage of the polymerization in which only species with high conversion x_l are present. An additional case (EX. 4) was simulated by adding a Normal-Logarithmic mode [Eq. (18)] of pure polystyrene particles, with average diameter 150 nm, standard deviation 0.1 and number concentration 0.75, to the case of EX. 2. This kind of PSD is normally obtained in miniemulsion polymerizations that exhibit simultaneous polymerization by homogeneous nucleation, thus producing a population of polymer particles of small diameters.

For each simulated example, the global PSD was obtained according to Eq. (7), as follows:

$$f(D_i) = \sum_{l=0}^{9} c_l \, g_l(D_i) \tag{21}$$

Figure 3a) compare the global PSDs $f_1(D_i)$, $f_2(D_i)$, $f_3(D_i)$ and $f_4(D_i)$ for examples EX. 1, EX.2, EX. 3 and EX. 4, respectively.

	c_0	c_1	c_2	c_3	c_4	c_5	c_6	c_7	c_8	c_9
EX. 1	0.50	0.25	0.15	0.10	0.0	0.0	0.0	0.0	0.0	0.0
EX. 2	0.05	0.05	0.05	0.10	0.25	0.25	0.10	0.05	0.05	0.05
EX. 3	0.00	0.00	0.00	0.00	0.00	0.00	0.10	0.15	0.25	0.50
EX.4	0.0125	0.0125	0.0125	0.025	0.0625	0.0625	0.025	0.0125	0.0125	0.875

Table 1: Number concentration of the different species in the four analyzed examples.
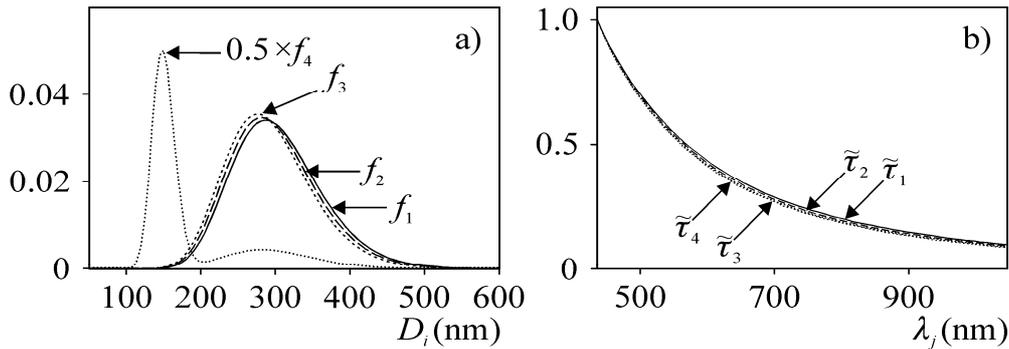
Figure 3: Global PSDs f_1, f_2, f_3 and f_4 (a) and noisy T measurements $\tilde{\tau}_1$, $\tilde{\tau}_2$, $\tilde{\tau}_3$ and $\tilde{\tau}_4$ (b) for the four analyzed examples

For simulating the T measurement, λ_j was assumed within the range [436 nm – 1046 nm] at regular intervals of 10 nm. The PRI of each simulated species, $n_{p,l}(\lambda_j,x)$ ($l = 0, …, 9$), was calculated through Eqs. (9a), (9b) and (10), on the basis of the corresponding conversions x_l, and the PRI of styrene (Kasarova et al., 2007) and polystyrene (Inagaki et al., 1977). The T measurements $\tau_1(\lambda_j)$, $\tau_2(\lambda_j)$, $\tau_3(\lambda_j)$ and $\tau_4(\lambda_j)$ were calculated on the basis of Eq. (6), as follows:

$$\boldsymbol{\tau} = k_\tau \sum_{l=0}^{9} \mathbf{Q}_l \, c_l \, \mathbf{g}_l \tag{22}$$

where $\mathbf{Q}_l$ (J×I) is the matrix with components $Q_{ext}[D_i, \lambda_j, n_m(\lambda_j), n_{p,l}(\lambda_j,x)] \, D_i^2$. For simulating examples representative of practical applications, all measurements were contaminated with random noise, as follows:

$$\tilde{\boldsymbol{\tau}} = \boldsymbol{\tau} + \sigma_\varepsilon \, \boldsymbol{\varepsilon} \tag{23}$$

where the oversymbol "~" indicates a noisy measurement; $\boldsymbol{\varepsilon}$ is a Gaussian random sequence of zero mean and unity standard deviation; and $\sigma_\varepsilon = 0.001 \times \max(\boldsymbol{\tau})$ is the standard deviation of the noise. Figure 3b) compares the simulated noisy measurements $\tilde{\tau}_1(\lambda_j)$, $\tilde{\tau}_2(\lambda_j)$, $\tilde{\tau}_3(\lambda_j)$ and $\tilde{\tau}_4(\lambda_j)$.

The global conversions x_1, x_2, x_3 and x_4 for examples EX. 1, EX. 2, EX. 3 and EX. 4, respectively, were assumed to be known and were calculated as:

$$x = \frac{\sum_{l=0}^{9} x_l \left(c_l \sum_{i=1}^{I} D_i^3 \, g_l(D_i) \right)}{\left(c_l \sum_{i=1}^{I} D_i^3 \, g_l(D_i) \right)} \tag{24}$$

Finally, the proposed method of section 2 was applied for estimating the global PSD of examples EX. 1, EX. 2, EX. 3 and EX. 4 on the basis of $\tilde{\tau}(\lambda_j)$ and x. For implementing the estimation procedure a diameter axis from 10 nm to 700 nm at regular intervals of 12.5 nm was assumed. Results are presented in Fig. 4) and in Table 2. Figure 4 compares the true calculated global PSDs with its estimates obtained through the Tikhonov method and the GRNN. Table 2 presents the average diameter $\overline{D}_{1,0}$, $\overline{D}_{4,3}$, $\overline{D}_{6,5}$ and $\overline{D}_{6,3}$ calculated on the basis of the true and estimated global PSDs through Eq. (1).
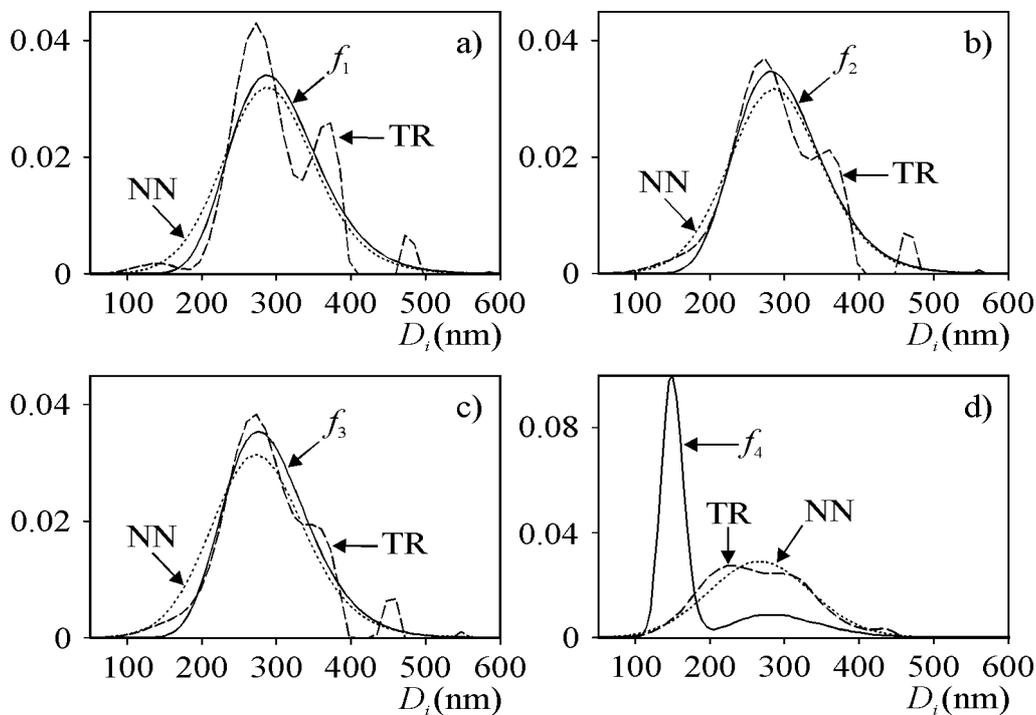

Figure 4: a-d) Simulated PSDs (*f*), and estimated through the Tikhonov regularization method (TR) and the GRNN (NN)

	$\overline{D}_{1,0}$ (nm)			$\overline{D}_{4,3}$ (nm)			$\overline{D}_{6,5}$ (nm)			$\overline{D}_{6,3}$ (nm)		
	True	TR	NN	True	TR	NN	True	TR	NN	True	TR	NN
EX. 1	305	299	294	330	325	324	372	367	370	358	352	354
EX. 2	299	291	291	324	320	321	365	364	365	351	349	350
EX. 3	293	287	280	318	315	312	358	360	361	344	345	344
EX. 4	188	264	268	252	319	302	351	339	343	321	326	329

Table 2: Average diameters calculated for the estimated PSDs

For unimodal PSDs (EX. 1, EX. 2 and EX. 3), both the Tikhonov method and the GRNN produce acceptable estimates of the average diameters exhibiting errors below 4%.

Additionally, the GRNN produces acceptable estimates of the global PSD although the left tail exhibited meaningful deviations [Fig. 4a-c]. On the contrary, the Tikhonov method produces PSDs with multiples erroneous spurious peaks. This is due the ill-conditioning of the inverse problem and may be overcome through a stronger regularization (a larger α). As an example, Fig. 5 compares the global PSD $f_1(D_i)$ with its estimates obtained through the Tikhonov regularization on the basis of $\alpha = 250$ (estimated by the L-curve method), $\alpha = 1000$, and $\alpha = 4000$. As expected, a larger α produced PSDs estimates without spurious modes. Table 3 compares the average diameters of the estimated PSDs. Note that the average diameters $\overline{D}_{6,5}$ and $\overline{D}_{6,3}$ remained almost constant for increasing α's.
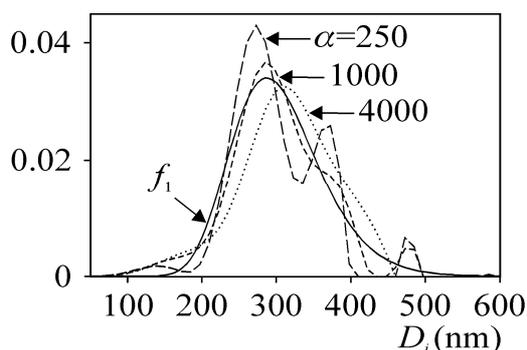

Figure 5: Comparison of PSD estimates obtained through the Tikhonov regularization with regularization parameter $\alpha = 250$ (estimated by the L-curve method), $\alpha = 1000$, and $\alpha = 4000$.

α	$\overline{D}_{1,0}$ (nm)		$\overline{D}_{4,3}$ (nm)		$\overline{D}_{6,5}$ (nm)		$\overline{D}_{6,3}$ (nm)	
	True	TR	True	TR	True	TR	True	TR
250		299		325		367		352
1000	305	301	330	328	372	366	358	353
4000		313		339		366		357

Table 3: Average diameters of the PSDs of Fig. 5.

In the particular case of EX. 4 both methods were incapable of acceptably recover the small diameter mode. This result is normally obtained in T, and is due the fact that the smaller particles have a low contribution to the T measurement than the larger particles. In general, most estimation methods normally produce erroneous estimation of populations of small particles. Additionally, for the case of the GRNN this result is expected since the training of the network was carried out with unimodal PSDs, and therefore, the output will always be unimodal. Note that although the average diameters $\overline{D}_{1,0}$ and $\overline{D}_{4,3}$ were erroneous, the $\overline{D}_{6,5}$ and $\overline{D}_{6,3}$ were acceptably estimated (Table 2).

4 CONCLUSIONS

A novel method based on turbidity measurements was proposed for on-line monitoring the particle size in miniemulsion polymerizations. The method involves solving an ill-conditioned inverse problem through two alternative approaches: a Tikhonov regularization method and a general regression neural network.

The proposed method was able to acceptably estimate the average diameters when samples

exhibit unimodal PSDs. Additionally, the neural network produced good estimates of the PSD. The Tikhonov method produced PSDs with erroneous spurious modes. For bimodal PSDs (typically obtained in reactions that also exhibit homogeneous nucleation) both methods produced erroneous PSD estimates. However, the proposed method was adequate to estimate the average diameters $\overline{D}_{6,5}$ and $\overline{D}_{6,3}$. Consequently, although the global PSD is erroneously recuperated in some applications, the proposed method could in principle be used for on-line monitoring the average diameter (either the $\overline{D}_{6,5}$ or the $\overline{D}_{6,3}$) along miniemulsion polymerizations. For example, along a miniemulsion polymerization only slight variations of the average diameter of the global PSD are observed; as can be seen in Table 2 where the $\overline{D}_{6,3}$ is 358 nm at the begining of the polymerization (EX. 1) and 344 nm at the end (EX. 3) (i.e. a variation of aproximately 4%). However, when the polymerization exhibits homogeneous nucleation (EX. 4) a meaningful decrease in the average diameters of the global PSD are produced. This can be seen in Table 2 where $\overline{D}_{6,3}$ is 321 nm for EX. 4 (i.e. a variation of almost 11% with respect to EX. 1). Thus, homogeneous nucleation along miniemulsion polymerization can be detected by monitoring the $\overline{D}_{6,5}$ and/or the $\overline{D}_{6,3}$.

With respect to the inversion techniques, although the neural network is less general because the estimated PSD is highly dependent of the selected training pattern utilized, the GRNN is a simple and fast technique that does not require previous expertise. On the contrary, the Tikhonov method requires some level of expertise of the user and frequently the obtained PSD exhibits spurious modes due the highly ill-conditioning of the inverse problem.

ACKNOWLEDGMENTS

REFERENCES

Alb, A.M., Farinato, R., Calbick, J., Reed, W.F., Online Monitoring of Polymerization Reactions in Inverse Emulsions. *Langmuir*, 22: 831-840, 2006.

Alb. A.M., Reed, W.F., Simultaneous Monitoring of Polymer and Particle Characteristics during Emulsion Polymerization. *Macromolecules*, 41: 2406-2414, 2008.

Aster, R., Borchers B. and Thurber, C., *Parameter Estimation and Inverse Problems*. Elsevier Academic Press, USA, 2005.

Bohren, C. and Huffman, D., *Absorption and Scattering of Light by Small Particles*. Wiley, New York, 1983.

Brandolin, A., García-Rubio, L., Provder, T., Koeheler, M. y Kuo, C., in *Particle Size Distribution II. Assessment and Characterization* (Ed. T. Provder), ACS Symposium Series No. 472, American Chemical Society, Washington D.C., 20, 1991.

Çatalgi-Giz, H., Giz, A., Alb., A.M., Reed. W.F., Absolute Online Monitoring of Acrylic Acid Polymerization and the Effect of Salt and PH on Reaction Kinetics. *J. Appl. Pol. Sci.*, 91(2): 1352-1359, 2003.

Chicoma, D.L., Sayer, C., Giudici, R., In-line Monitoring of Particle Size During Emulsion Polymerization Under Different Operational Conditions Using NIR Spectroscopy. *Macr. Reac. Eng.*, 5: 150-162, 2011.

Gugliotta, L., Clementi L., Vega, J., in *Measurement of Particle Size Distribution of Polymer Latexes*. Research Signpost, Kerala, India, 2010.

Hansen, P.C. y O'Leary, D.P., The Use of the L-curve in the Regularization of Discrete Ill-posed Problems. *SIAM J. Sci. Comput.*, 14: 1487-1503, 1993.

Hansen, P.C., Regularization Tools: A Matlab Package for Analysis and Solution of Discrete Ill-posed Problems. *Numerical Algorithms*, 6: 1-35, 1994.

Haykin, S., *Neural Networks: A Comprehensive Foundation*, 2nd Ed. Prentice Hall, New Jersey, 1999.

Higgins, J.P., Arrivo, S.M., Thurau, G., Green, R.L., Bowen, W., Lange, A., Templeon, A.C., Thomas, D.L., Reed, R.A., Spectroscopic Approach for On-line Monitoring of Particle Size during the Processing of Pharmaceutical Nanoparticles. *Anal. Chem.*, 75: 1777-1785, 2003.

Inagaki T., Arakawa E.T., Hamm R.N., y Williams M.W., Optical Properties of Polystyren from the Near Infrared to the X-Ray Region and Convergence of Optical Sum Rules. *Physical Review*, 6 (15): 3243, 1977.

Iulian, O., Stefaniu, A., Ciocirlan, O., Fedeles, A., Refractive Index in Binary and Ternary Mixtures With Diathylene Glycol, 1,4-Dioxane and Water Between 293.15-313.15 K. *U.P.B. Sci. Bull., Series B*, 72 (4): 37-44, 2010.

Kasarova, S.N., Sultanova, N.G., Ivanov, C.D., Nikolov, I.D., Analysis of the Dispersion of Optical Plastic Materials. Optical Materials, 29: 1481-1490, 2007.

Kiparissides, C., MacGregor, J.F., Singh, S., Hamielec, A.E., Continuous Emulsion Polymerization of Vinyl Acetate. Part. III: Detection of Reactor Performance by Turbidity-Spectra and Liquid Exclusion Chromatography. *Canadian Journal of Chemical Engineering*, 58: 65-71, 1980.

Minari R., Goikoetxea M., Beristain I., Paulis M., Barandiaran M., Asua J., Post-polymerization of Waterborne Alkyd/Acrylics. Effect on Polymer Architecture and Particle Morphology. *Polymer*, 50: 5892-5900, 2009.

Ronco L.I., Minari, R.J., Vega, J.R., Meira, G.R., Gugliotta, L.M, Incorporation of Polybutadiene into Waterborne Polystyrene Nanoparticles via Miniemulsion Polymerization. *European Polymer Journal*, 2013 (In Press).

Schork, J.F., Luo, Y., Smulders W., Russum J.P, Butte A., Fontenot K., Miniemulsion Polymerization. *Adv. Polym. Aci.*, 175: 129-155, 2005.

Specht, D.F., A General Regression Neural Network. *IEEE Transactions on Neural Networks*, 2(6): 568-576, 1991.

Specht, D.F., The General Regression Neural Network-Rediscovered. *Neural Networks*, 6(7): 1033-1034, 1993.

Tikhonov A., and Arsenin, V. *Solution of Ill-posed Problems*. Wiley, New York, 1977.

Zhong, M., Goggeshall, D., Ghaneie, E., Pope, T., Rivera, M., Georgiopoulos, M., Anagnostopoulos, G., Mollaghasemi, M. y Richie, S., *Gap-Based Estimation: Choosing the Smoothing Parameters for Probabilistic and General Regression Neural Networks*, National Sciene Foundation, Florida, Orlando, USA, 2005.